

Achieving high durability in all-solid-state lithium metal batteries using metal–organic framework solid polymer electrolytes

Suin Kim,^{a,b†} Hasan Jamal,^{a‡}, Firoz Khan,^c Amir Al-Ahmed,^c Mahmoud M. Abdelnaby,^d

Atif Al-Zahrani,^c Sang-Eun Chun,^{b*} and Jae Hyun Kim^{a**}

^aDivision of Energy Technology, Daegu Gyeongbuk Institute of Science & Technology, 333, Techno Jungang-Daero, Hyeonpung-Myeon, Dalseong-Gun, Daegu 42988, Republic of Korea.

^bSchool of Materials Science and Engineering, Kyungpook National University, Daegu, 41566, Republic of Korea

^cInterdisciplinary Research Center for Sustainable Energy Systems (IRC-SES), King Fahd University of Petroleum and Minerals (KFUPM), Dhahran 31261, Saudi Arabia

^dInterdisciplinary Research Center for Hydrogen and Energy Storage (IRC-HES), King Fahd University of Petroleum and Minerals (KFUPM), Dhahran 31261, Saudi Arabia

[†]These authors contributed equally to the work.

^{*}Corresponding author.

^{**}Corresponding author.

E-mail addresses: sangeun@knu.ac.kr (S.E. Chun), jaehyun@dgist.ac.kr (J.H. Kim)

Supplementary content

1. Synthesis of ZR8 MOF
2. Materials characterization
3. Electrochemical characterization
4. Fabrication of cathode
5. Degree of crystallinity calculation from DSC data
6. Calculation of Li-ion transference number
7. Tables
8. Figures

Synthesis of ZR8 MOF

The detailed procedure of the synthesis of ZR8-MOF is already reported somewhere else.¹ Zirconium tetrachloride (ZrCl_4 , 1.05 g, 4.5 mmol) was dissolved in 99.5 % acetic acid solution of 45 ml, while benzene-1,3,5-tricarboxylic acid (BTC, 0.31 g, 1.5 mmol) was dissolved in dimethylformamide (DMF) using ultrasonication for 30 minutes. After sonication, the ZrCl_4 and BTC solutions were combined and heated to 120 °C for a specific duration (e.g., 36-96 h) in a Teflon-lined high-pressure reactor. The molar ratio of ZrCl_4 to BTC was maintained between (0.5-3/1). The resulting reaction product was washed four times with acetone, followed by drying at 100 °C for 12 hours. Subsequently, the sample was activated in chloroform (CHCl_3) for three days at 50 °C, with daily replacement of CHCl_3 . Finally, the sample was dried under vacuum at 120 °C for 24 hours to obtain the MOF-808 samples. To produce the optimized ZR8-MOF sample, a reaction temperature of 120 °C, a ZrCl_4/BTC ratio of 3:1, and a reaction time of 72 hours were used.

Materials characterization

Universal testing machine (United Calibration, SFM-100kN) was measured the stress-strain scales of the CPE. Differential scanning calorimetry (DSC, Q2000 TA Instruments) investigated the phase transition behavior. However, thermal stability was examined using Thermo-gravimetric analysis (TGA, Q500 TA Instruments). An X-ray diffractometer (XRD, Empyrean-Malvern Panalytical) was used to study the structural properties from using Cu K α radiation. The morphological was carried out using Field emission scanning electron microscopy (FE-SEM, Hitachi, S-4800). The chemical bonding analysis was done using X-ray photoelectron spectrometry (XPS, M/s Thermo Scientific, ESCALAB 250Xi). Raman spectra were recorded on a 780 nm in Via Raman microscope spectrometer (Raman, Thermo Scientific/Nicolet Almega XR). The heat release rate (HRR) was measured using a micro combustion calorimeter (MCC, Fire testing technology, FTT0001). The HRR measurement was conducted on a 15 mg sample at a heating rate of approximately 1 °C s⁻¹, within the 150-800 °C temperature range. The gas used for the experiment was a mixture of N₂ and O₂ in an 80:20 ratio.

Electrochemical characterization

The electrochemical characterization was performed by using a battery cycler (WBCS3000, WonATech), and a potentiostat (ZIVE MP1, WonATech). The cells were activated at 70 °C for 2 hours before each electrochemical measurement to ensure good contact between the electrodes and electrolytes.

The ionic conductivities of the CPEs in the temperature range of 20 to 70 °C were measured by electrochemical impedance spectroscopy (EIS) in the frequency range of 2 MHz to 50 mHz, with an applied amplitude of 5 mV. The ionic conductivities (in S cm⁻¹) of the CPEs were calculated using [Eq. \(S1\)](#),

$$\sigma = \frac{L}{R \times S} \quad (\text{S1})$$

where R (in Ω) is the value of charge transfer resistance extracted from the Nyquist plot, L (in cm) is the thickness of the electrolyte film, and S (in cm²) is the cross-sectional area of the electrolyte film, respectively. Before each measurement, the stainless steel (SS) symmetric cell (SS/CPE/SS) was thermally stabilized for 2 hours.

The electrochemical stability of the ZR8-CPE was investigated by linear sweep voltammetry (LSV), which was conducted at a scan rate of 0.1 mV s⁻¹ in a voltage range of 2.6 to 6.0 V (vs. Li/Li⁺). The lithium-ion transference number (t_{Li^+}) of the ZR8-CPE was determined by chronoamperometry, based on the DC polarization and AC impedance. DC polarization voltage of 10 mV was applied to the cell to measure the initial and steady currents and Nyquist plots before and after DC polarization were obtained by AC impedance spectroscopy. Lithium stripping deposition cycling was performed to investigate the influence of ZR8-CPE on the electrochemical performance of Lithium metal anode. Galvanostatic cycling were performed

within the potential window of 2.6 to 4 V. The LFP/CPE/Li half-cell was cycled by using CR2032 coin cell to investigate the cycle stability and rate performance.

Fabrication of cathode

A composite cathode was synthesized by mixing active material, conductive carbon, binder and solid-polymer electrolyte (SPE) to strengthen the contact between the CPE and the electrode. These materials weight ratio of LFP, Super P, carbon nanotube, polyvinylidene fluoride (PVDF), LiTFSI and PEO was 75:8:1:4:3:9 wt%, respectively. Whole ingredient was dissolved in N-Methyl-2-pyrrolidone (NMP) and mixed using high energy ball-milling machine. The uniformly mixed slurry was casted on Al-foil by using doctor blade technique. After drying the composite cathode in convention oven at 90 °C for 2 hours followed by in vacuum oven at 70 °C for 12 hours. The loading mass of composite cathode was 2 mg cm⁻².

Degree of crystallinity calculation from DSC data

DSC data were secured for phase transition behavior of the ZR8-CPE including glass transition temperature (T_g), melting temperature (T_m), enthalpy of melting (ΔH_m) and degree of crystallinity (X_c). The degree of crystallinity (X_c) is calculated using [Eq. \(S2\)](#),

$$x_c \equiv \frac{\Delta H_m}{\Delta H_0} \quad (S2)$$

Where, ΔH_m was obtained from DSC results, and ΔH_0 is the melting enthalpy of 100% crystalline PEO (213.7 J g^{-1}).^{2,3}

Calculation of Li-ion transference number

The determination of the Li-ion transference number (t_{Li}^+) is crucial in solid-state electrolytes (SSEs) as it offers valuable insights into the anion movement during charge-discharge cycling. This parameter plays a significant role in the polarization of the electrolyte throughout the cycling process. The t_{Li}^+ of the ZR8-CPEs was evaluated using the Bruce-Vincent equation (Eq. S3). To measure the t_{Li}^+ of the ZR8-CPEs, a symmetric [Li|ZR8-CPEs|Li] cell configuration was employed.

$$t_{Li^+} = \frac{I_s(\Delta V - I_0 R_0)}{I_0(\Delta V - I_s R_s)} \quad (S3)$$

To calculate t_{Li}^+ , the currents before (I_0) and after (I_s) polarization, as well as the resistance before (R_0) and after (R_s) polarization, are measured. Additionally, the DC voltage applied for polarization (ΔV) is considered. By comparing these parameters, it becomes possible to determine the t_{Li}^+ value, which reflects the proportion of Li^+ ions involved in charge transport.

Table S1. Composition of PEO, LiTFSI, and ZR8 dispersed in ACN (15 mL) for the synthesis of SPE and ZR8-CPEs.

Sample name	PEO (g)	LITFSI (g)	ZR8 (g)
SPE	0.4	0.16	0
ZR8-2.5	0.4	0.16	0.014
ZR8-5.0	0.4	0.16	0.028
ZR8-7.5	0.4	0.16	0.042
ZR8-10	0.4	0.16	0.056

Table S2. DSC data for phase transition behavior of SPE and ZR8-CPEs including the values of melting temperature (T_m), melting enthalpy (ΔH_m) and crystallinity (X_c).

Sample name	T_m (°C)	ΔH_m (J g ⁻¹)	X_c (%)
SPE	49.18	50.417	23.59
ZR8-2.5	48.47	41.724	19.52
ZR8-5.0	44.68	41.477	19.41
ZR8-7.5	42.49	36.209	16.94
ZR8-10	48.4	48.371	22.64

Table S3. TGA data of SPE and ZR8-CPEs decomposition temperature and the weight

Sample name	Decomposition temperature (°C)	Weight remaining after 800 °C (%)
SPE	335.63	2.51
ZR8-2.5	328.38	3.09
ZR8-5.0	323.71	3.53
ZR8-7.5	318.34	5.37
ZR8-10	285.38	6.44

remaining after 800°C values.

Table S4. Heat release rate (HRR), Heat release capacity (HRC), and Heating rate parameters obtained from the microcalorimetry flame testing equipment.

Sample name	HRR (W g^{-1})	HRC ($\text{J g}^{-1} \text{K}^{-1}$)	Heating rate ($^{\circ}\text{C s}^{-1}$)
SPE	436	473	~1
ZR8-2.5	411	447	~1
ZR8-5.0	327	365	~1
ZR8-7.5	297	319	~1
ZR8-10	282	308	~1

Table S5. Parameter of ZR8-CPE's tensile test.

Sample name	Stress (MPa)	Strain (%)
ZR8-2.5	2.45	221.94
ZR8-5.0	2.55	238.23
ZR8-7.5	2.61	246.62
ZR8-10	2.89	229.07

Table S6. Raman data for ratio of free-ions and cluster-ions.

Sample name	Peak area of TFSI ⁻ (740.14 cm ⁻¹)	Peak area of [Li(TFSI) ₂] ⁻¹ (745.89 cm ⁻¹)	Total peak area	% of [Li(TFSI) ₂] ⁻¹
SPE	4588.38	773.45	5361.82	14.43
ZR8-2.5	5580.47	705.08	6285.54	11.22
ZR8-5.0	6690.32	650.42	7340.77	8.86
ZR8-7.5	3453.96	272.6	3726.56	7.32
ZR8-10	5961.12	840.62	6801.80	12.36

Table S7. Ionic conductivities of ZR8-CPEs, measured at various temperatures (20, 30, 40, 50, 60, and 70 °C).

Sample	σ (S cm ⁻¹)					
	20 °C	30 °C	40 °C	50 °C	60 °C	70 °C
ZR8-2.5	6.52×10^{-5}	9.31×10^{-5}	1.23×10^{-4}	5.45×10^{-4}	6.65×10^{-4}	1.24×10^{-3}
ZR8-5.0	7.98×10^{-5}	1.24×10^{-4}	1.81×10^{-4}	5.94×10^{-4}	1.08×10^{-3}	1.67×10^{-3}
ZR8-7.5	1.20×10^{-4}	2.53×10^{-4}	3.63×10^{-4}	7.77×10^{-4}	1.35×10^{-3}	2.79×10^{-3}
ZR8-10	3.46×10^{-5}	1.17×10^{-4}	1.82×10^{-4}	3.26×10^{-4}	6.33×10^{-4}	7.38×10^{-4}

Table S8. The parameter used for the determination of t_{Li^+} for ZR8-CPEs at 60 °C.

Sample	I_0 (μA)	I_s (μA)	R_0 (Ω)	R_s (Ω)	ΔV (V)	t_{Li^+}
ZR8-2.5	27.95	22.52	33.123	396.60	0.01	0.56
ZR8-5.0	40.02	27.46	144.21	201.63	0.01	0.65
ZR8-7.5	23.53	20.21	327.89	354.70	0.01	0.69
ZR8-10	28.91	23.61	239.54	248.91	0.01	0.61

Table S9. Overpotential values of ZR8-CPEs at various current densities in lithium plating/stripping analysis

Sample	Voltage (V)				
	50 $\mu\text{A cm}^{-2}$	100 $\mu\text{A cm}^{-2}$	200 $\mu\text{A cm}^{-2}$	300 $\mu\text{A cm}^{-2}$	300 $\mu\text{A cm}^{-2}$ (234 th hour)
ZR8-2.5	0.023	0.054	0.11	0.22	0.21
ZR8-5.0	0.019	0.052	0.127	0.387	0.167
ZR8-7.5	0.016	0.041	0.078	0.117	0.113
ZR8-10	0.047	0.125	0.273	0.269	0.428

Table S10. The comparison of t_{Li^+} values and plating/stripping results with the published reports.

Electrolyte	Ionic conductivity (S cm^{-1})	Current density ($\mu\text{A cm}^{-2}$)	Stripping time (h)	WT (°C)	t_{Li^+}	Ref.
PEO- LiTFSI- SiO ₂ /TDI*	1.2×10 ⁻⁴ @25 °C 0.14×10 ⁻² @60 °C	0.05	1000	60	0.33	4
PEO-LiTFSI- SNWs***	2.52×10 ⁻⁴ @40 °C 1.01×10 ⁻³ @80 °C	0.1	800	50	0.22	5
PEO-LiTFSI-(Ca- CeO ₂) [□]	1.3×10 ⁻⁴ @60 °C	0.1	1000	60	0.45	6
PEO-LiTFSI- LLZO	1.5×10 ⁻⁴ @35 °C	0.1	1500	55	0.49	7
PEO-LiClO ₄ -SiO ₂	1.1×10 ⁻⁴ @30 °C	0.1	400	90	0.367	8
PEO-LiClO ₄ -SiO ₂	1.1×10 ⁻⁴ @ 30 °C	0.1	400	55	NA	9
PEO- LiTFSI- SBA [€] /LiIL [§]	4.3×10 ⁻⁴ @60 °C	0.1	200	60	NA	10
PEO-LiTFSI- MZLT [◊]	5.74×10 ⁻⁴ @30 °C	0.1	1800	60	0.83	11
PEO-LiTFSI- PTFE [®]	1.40×10 ⁻³ @30 °C	0.1	900	60	NA	12
PEG-PEI- LiTFSI-MOF	3.01× 10 ⁻⁵ @30 °C	0.1	1000	60	0.54	13
P@CMOF	6.3 × 10 ⁻⁴ @60 °C	0.1	400	60	0.72	14
PL-10M	2.3 × 10 ⁻⁴ @30 °C	0.1	1400	50	0.66	15
SCE-MIL [□]	2.14 × 10 ⁻⁴ @60 °C	0.1	800	60	0.234	16
CSPE-Ce- MOF [□]	3.1 × 10 ⁻⁴ @60 °C	0.1	1800	60	0.75	17
ZR8-7.5	1.35 × 10⁻³	0.1	8000	60	0.69	Our work

WT = working temperature and t_{Li^+} = Li-ion transference number

* TDI = 2,4 -toluene diisocyanate

§ LiIL = Li-ion containing ionic liquid

** SNts = One-dimensional silica nanotubes

*** SNWs = SiO₂ nanowires

€SBA= Mesoporous silica

◊ MUSiO₂ = Monodispersed ultrafine SiO₂ nanospheres

□SCE-MIL = MIL-100 (Fe) solid composite electrolyte

□CSPE-MOF = Ce-based MOF solid polymer electrolyte

◊LLZO = Li₇La₃Zr₂O₁₂

△LGPS = Li₁₀GeP₂S₁₂

◊MZLT = A hydrophobic surface-modified zeolite filler

Table S11. Discharge capacity values of ZR8-CPEs with LFP from 0.1-1 C at 60 °C.

Sample	Capacity (mAh g ⁻¹)				
	0.1 C	0.2 C	0.5 C	1 C	0.2 C
ZR8-7.5	151.0	147.5	145.0	139.7	157.2

Table S12. 1st, last cycle discharge capacity, and capacity retention (%) with LFP at charging rate of 0.2 C and discharge rate of 0.5 C at 60 °C.

Sample	1 st capacity (mAh g ⁻¹)	Maximum capacity (mAh g ⁻¹)	Last capacity (mAh g ⁻¹)	Capacity retention (%)
ZR8-2.5	140.4	143.50	97.6	71.40
ZR8-5.0	142.2	142.98	110.49	77.77
ZR8-7.5	144.9	145.5	116.7	80.53
ZR8-10	141.0	143.3	99.6	70.63

Table S13. Comparison of electrochemical performance of composite polymer electrolytes-based Li-metal solid-state batteries.

Electrolyte	Cathode/Anode	WV (V)	SC (mAh g ⁻¹)	RR (%)	WT (°C)	LW (mg cm ⁻²)	Ref.
PEO-LiTFSI-SiO ₂ /TDI*	LiFPO ₄ /Li	2.7-3.8	150	83.7 (200) 0.2 C	60	NA	4
PEO-LiTFSI-SNts**	LiFPO ₄ /Li	2.8-4.2	151	83.4 (100) 0.1 C	60	3.8	18
PEO-LiTFSI-SNWs***	LiFPO ₄ /Li	2.4-4.0	122	89.3 (50) 0.5 C	50	1.6	5
PEO-LiTFSI-(Ca-CeO ₂) [□]	LiFPO ₄ /Li	2.5-4.0	125	74.4 (200) 1.0 C	60	NA	6
PEO-LiTFSI-LAGP [□]	LiFPO ₄ /Li	2.5-3.8	145	92.0 (300) 0.5 C	60	4	19
PEO-LiTFSI-LLZO	LiFPO ₄ /Li	2.8-3.8	155	84.0 (450) 0.2 C	55	NA	7
PEO-LiTFSI-Li ₂ S ₆	LiFPO ₄ /Li	2.8-4.3	130	80.7 (400) ~0.3 C	50	NA	20
PEO-LiTFSI-ZYNa	LiFPO ₄ /Li	2.6-4.0	156	95.0 (100) 0.1 C	60	2.2-2.5	21
PEO-LiClO ₄ -SiO ₂	LiFPO ₄ /Li	2.5-4.3	88	62.8 (10-100) 0.2 C	90	7	8
PEO-LiClO ₄ -MUSiO ₂ [⊖]	LiFPO ₄ /Li	2.5-4.1	130	78.5 (65) 1 C	90	1	22
PEO-LiClO ₄ -SiO ₂	LiFPO ₄ /Li	2.7-3.9	140	67.8 (90) 0.2 C	60	1	9
PEO-LiTFSI - SiO ₂ /Li ₂ SO ₄	LiFPO ₄ /Li	2.7-3.9	140	57.1 (50) 0.5 C	60	1.2-1.5	23
PEO-LiTFSI-SBA [€] /LiIL [§]	LiFPO ₄ /Li	NA	140	85.7 (80) 0.1 C	60	NA	10
PEO-LiTFSI-LLZO [∞]	LiFPO ₄ /Li	2.8-4.2	160	97.4 (70) 0.5 C	60	1.68	24
PEO-LiTFSI-LGPS [▲]	LiFPO ₄ /Li	2.5-4.0	158	91.0 (150) 0.5 C	60	NA	25
PEO-LiTFSI-VAVS [^]	LiFPO ₄ /Li	2.5-3.7	130	82.0 (200) 0.5 C	35	0.8	26
PEO-LiTFSI-MZLT [○]	LiFPO ₄ /Li	2.6-4.0	119	98.5 (200) 0.5 C	60	2.5	11
PEO-LiTFSI-ZR8-7.5	LiFPO₄/Li	2.6-4	144.9	80.53 (800) 0.5 C	60	2	Our work

WV = working voltage, WT = working temperature, SC = specific capacity, RR = retention rate and LW = loading weight

* TDI = 2,4 -toluene diisocyanate

§ LiIL = Li-ion containing ionic liquid

** SNts = One-dimensional silica nanotubes

*** SNWs = SiO₂ nanowires

[€]SBA= Mesoporous silica

[⊖]MUSiO₂ = Monodispersed ultrafine SiO₂ nanospheres

[∞]LLZO= Li₇La₃Zr₂O₁₂

^ΔLGPS = Li₁₀GeP₂S₁₂

[⊖]MZLT = A hydrophobic surface-modified zeolite filler

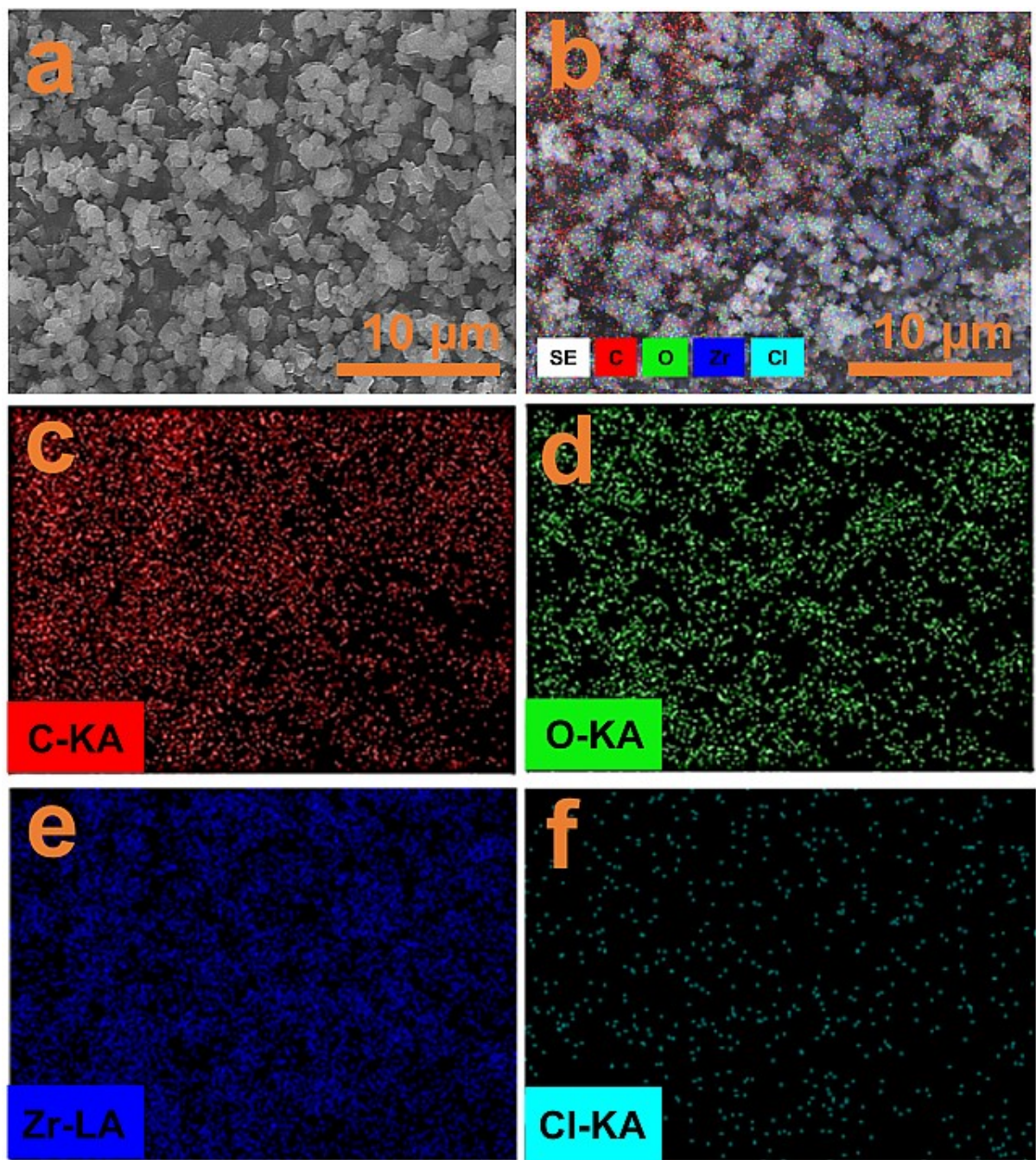


Fig. S1. The FE-SEM image and SEM-EDX mapping of ZR8 (a) SEM image, (b) overall mapping, (c) C (d) O (e) Zr, and (f) Cl element.

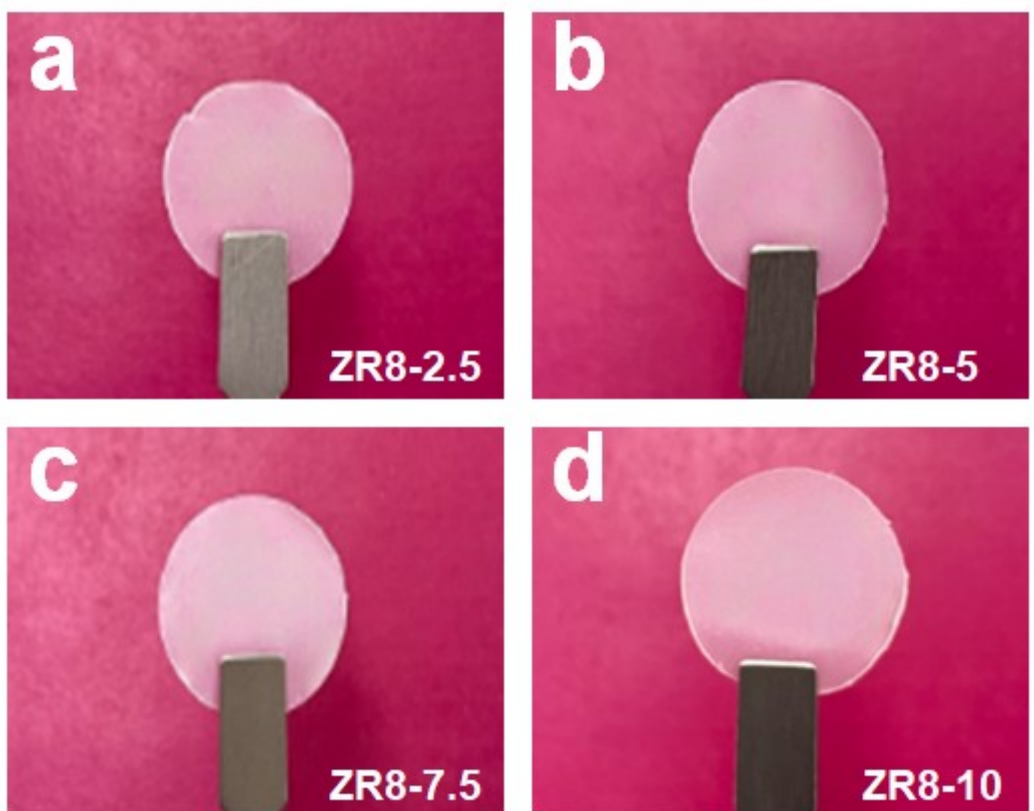


Fig. S2. The optical image of CPEs with different ZR8 contents: (a) 2.5 %, (b) 5 %, (c) 7.5 %, and (d) 10 %.

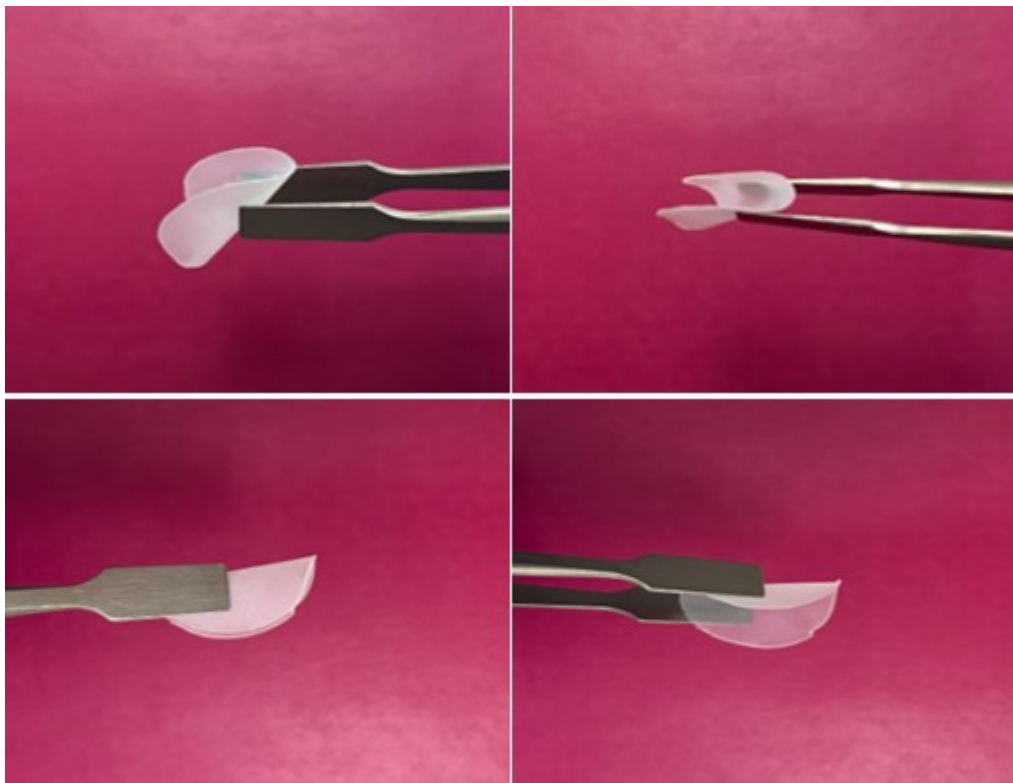


Fig. S3. Bending images at various angles of the ZR8-7.5.

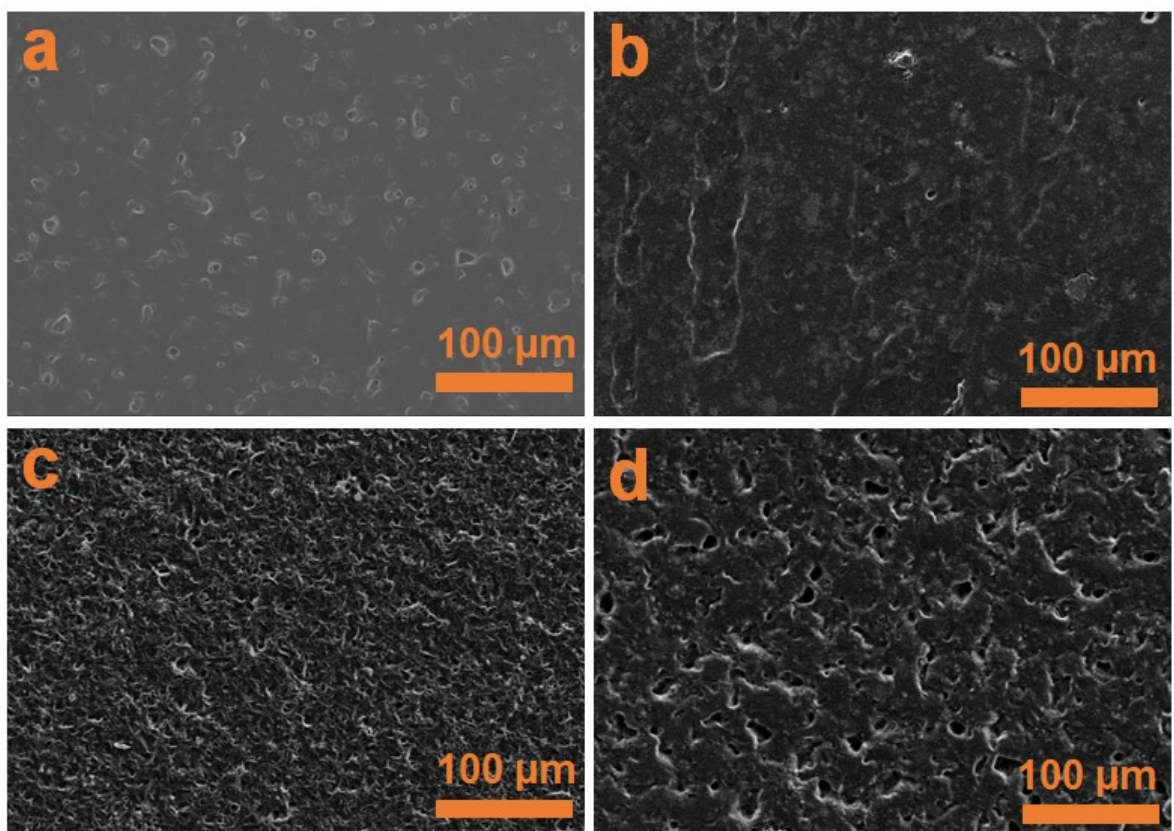


Fig. S4. SEM image of (a) ZR8-2.5, (b) ZR8-5, (c) ZR8-7.5, and (d) ZR8-10.

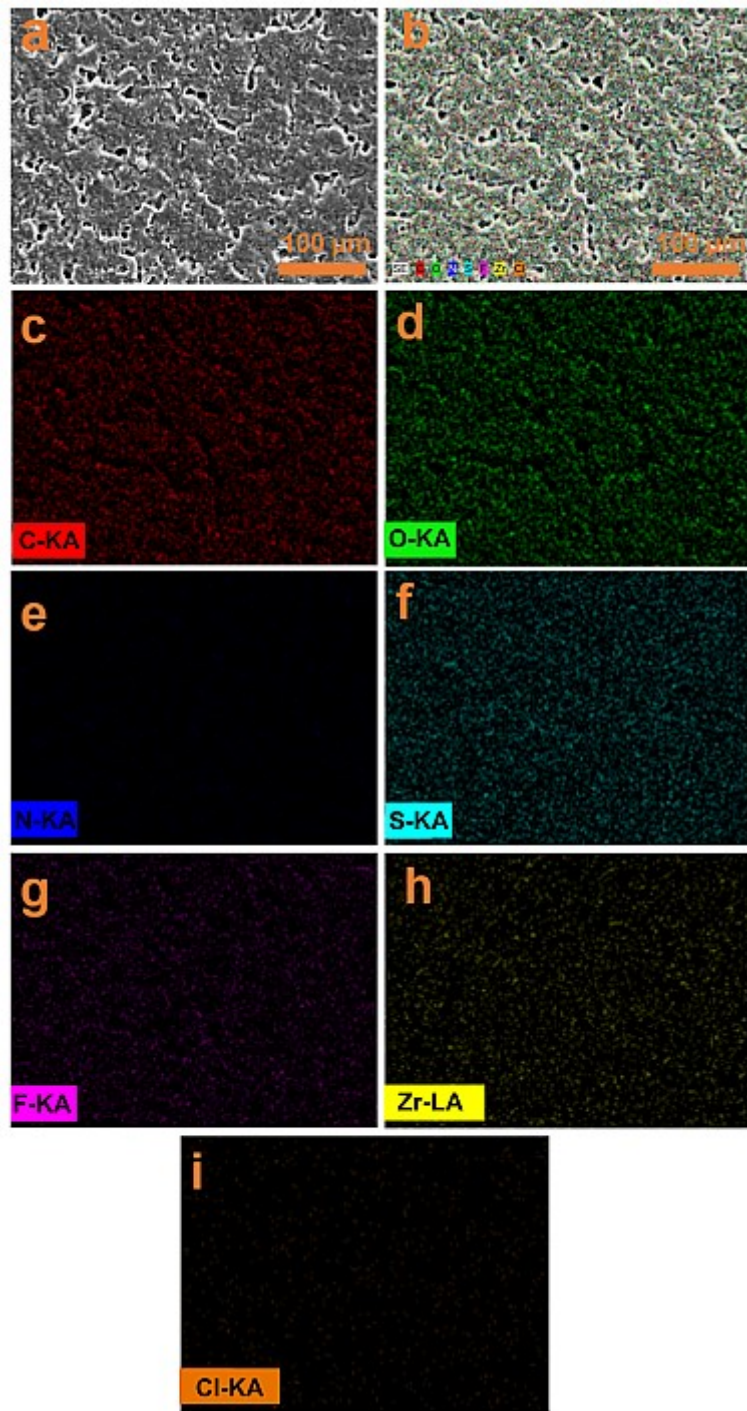


Fig. S5. The FE-SEM image and SEM-EDX mapping of ZR8-7.5 (a) SEM image, (b) overall mapping, (c) C (d) O (e) N, (f) S, (g) F, (h) Zr, and (i) Cl element.

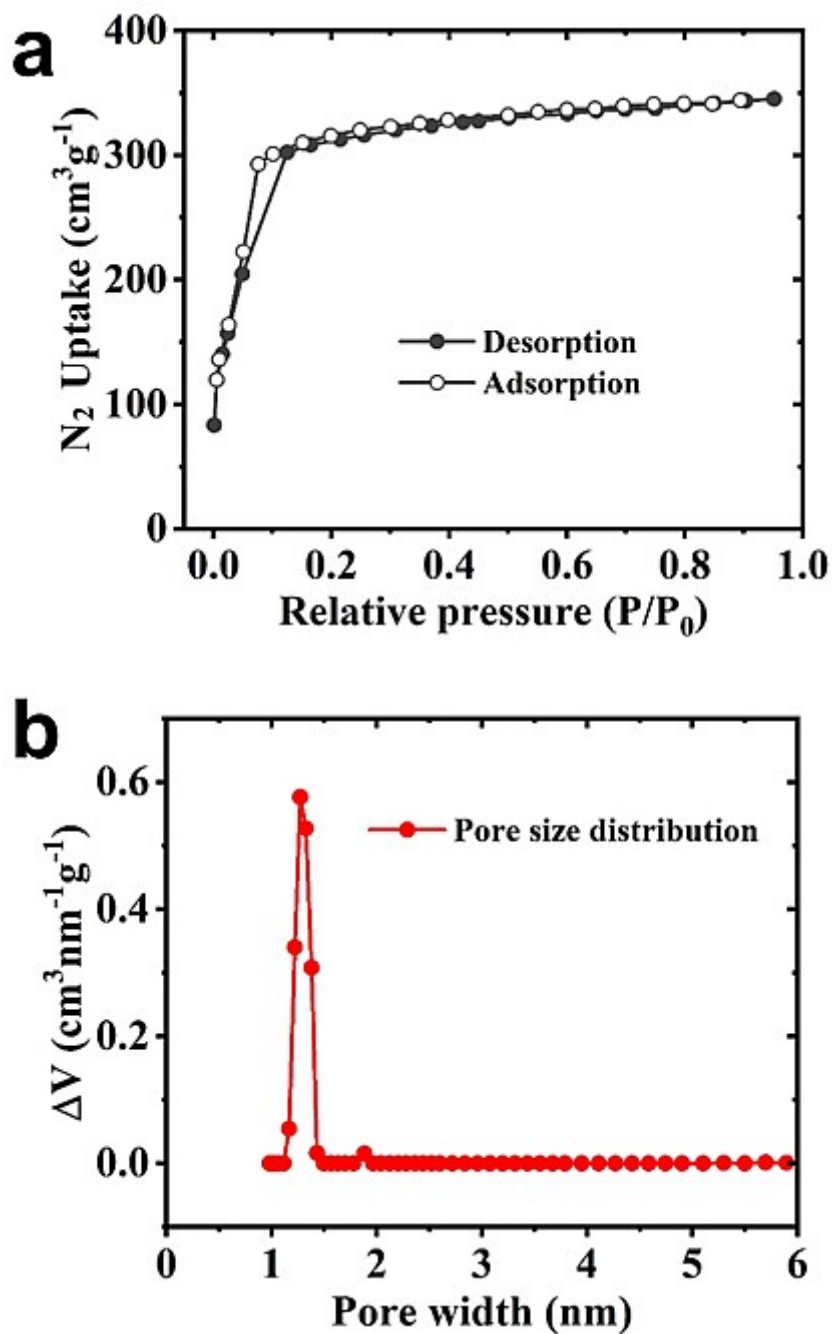


Fig. S6. (a) Nitrogen adsorption–desorption isotherms of ZR8. (b) Pore size distributions of ZR8.

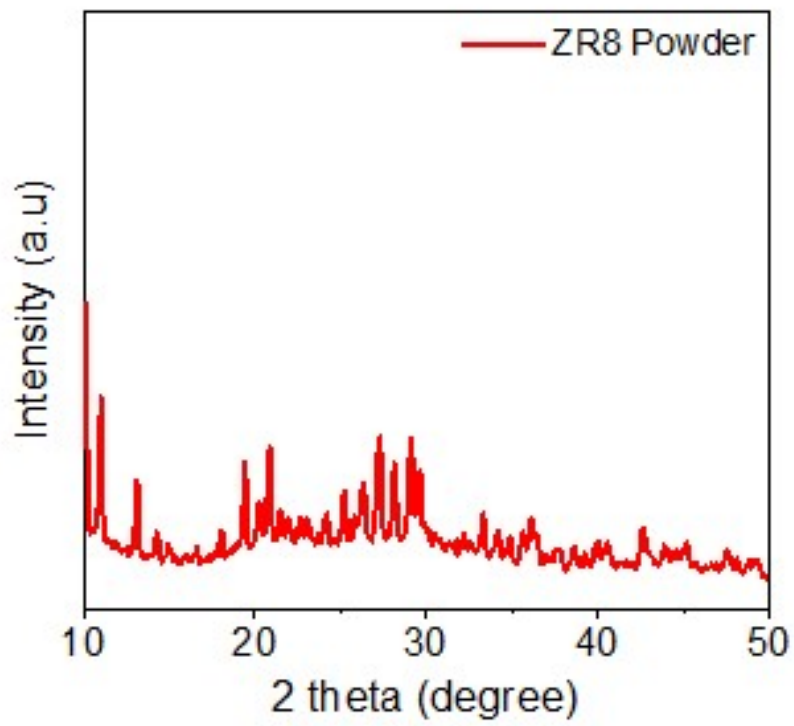


Fig. S7. XRD patterns of ZR8 powder from 10-50 °.

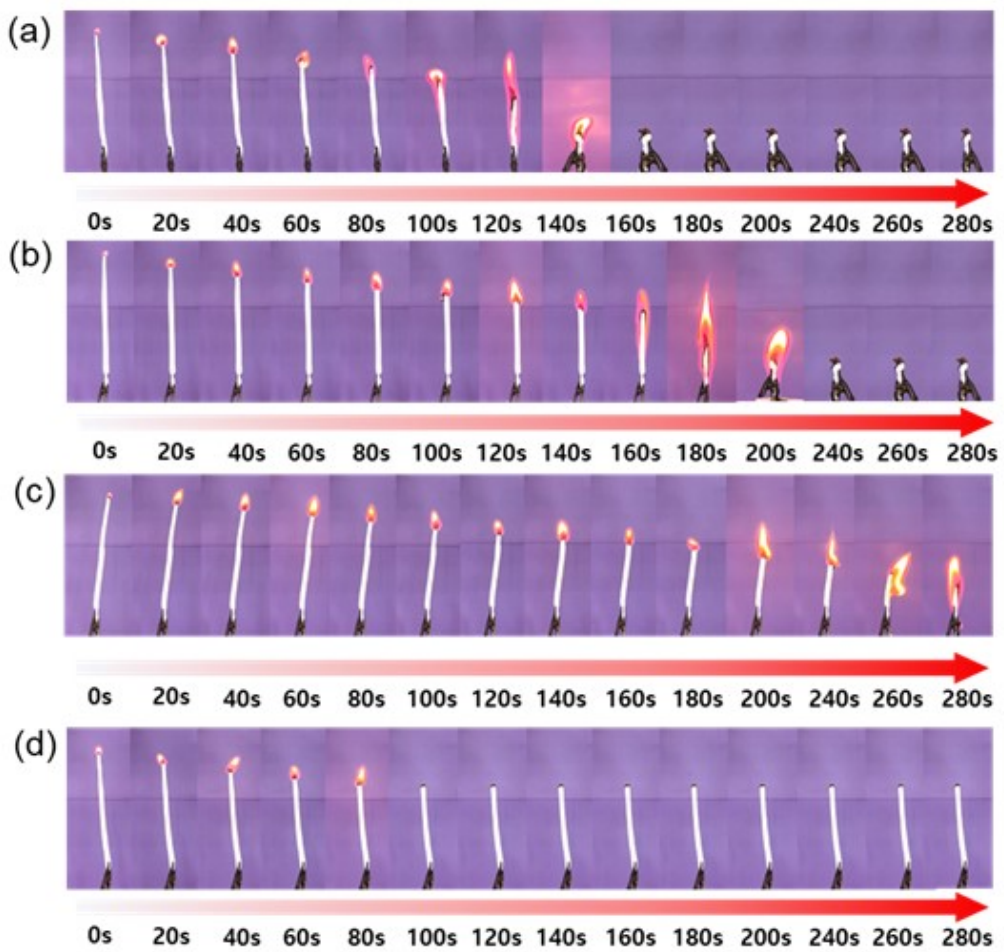


Fig. S8. Flame test of (a) ZR8-2.5, (b) ZR8-5, (c) ZR8-7.5, and (d) ZR8-10.

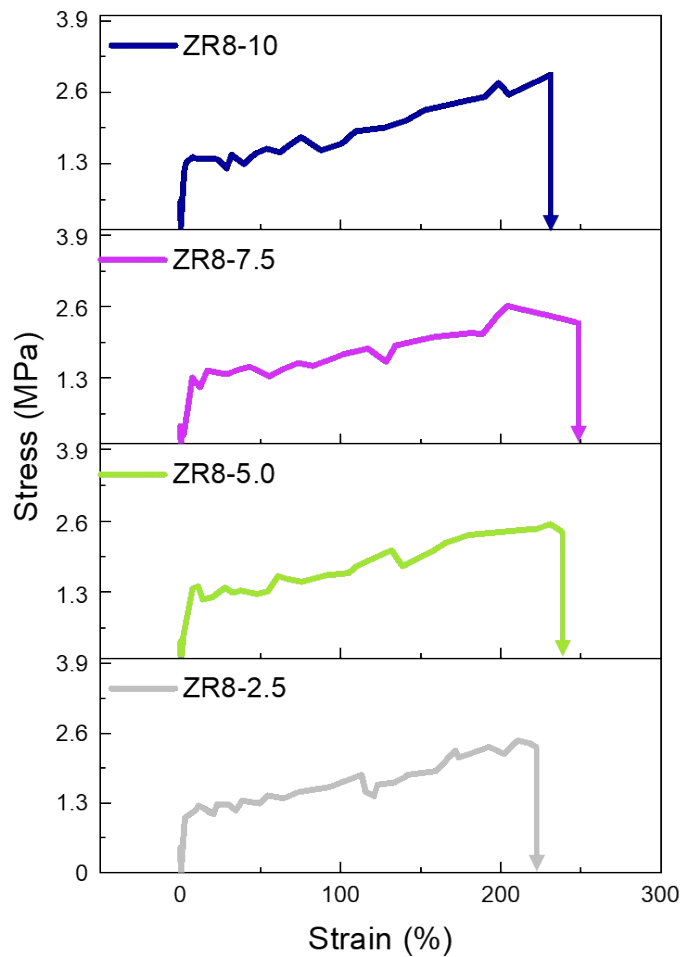


Fig. S9. Room Temperature Stress-Strain Curves of ZR8-CPEs with varying ZR8 Content (2.5-10%) at a scan rate of 10 mm min^{-1} .

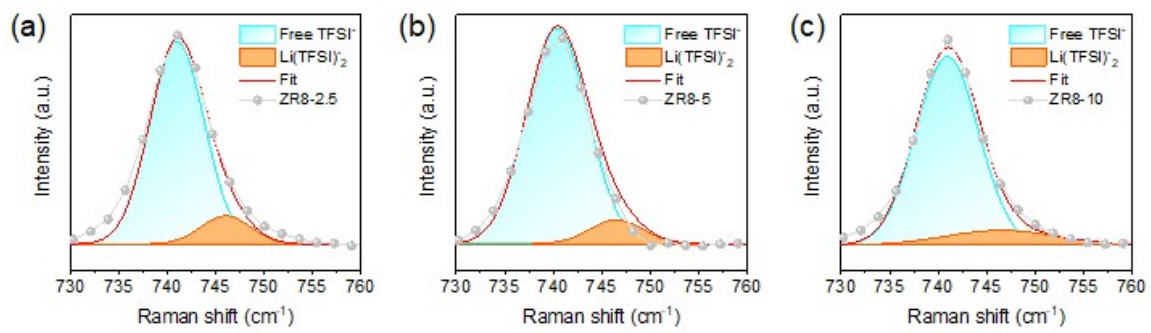


Fig. S10. Raman spectra of (a) ZR8-2.5, (b) ZR8-5, and (c) ZR8-10.

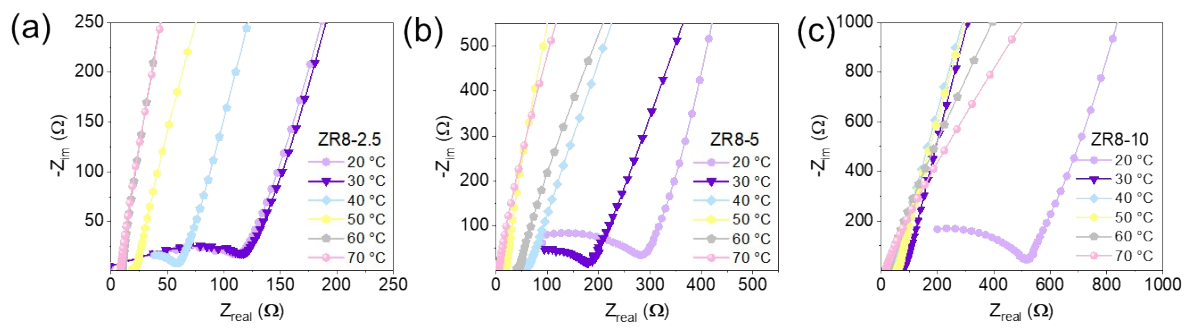


Fig. S11. Ionic conductivity study of ZR8-CPEs. The impedance spectra in the temperature range of 20-70 °C for (a) ZR8-2.5, (b) ZR8-5, and (c) ZR8-10.

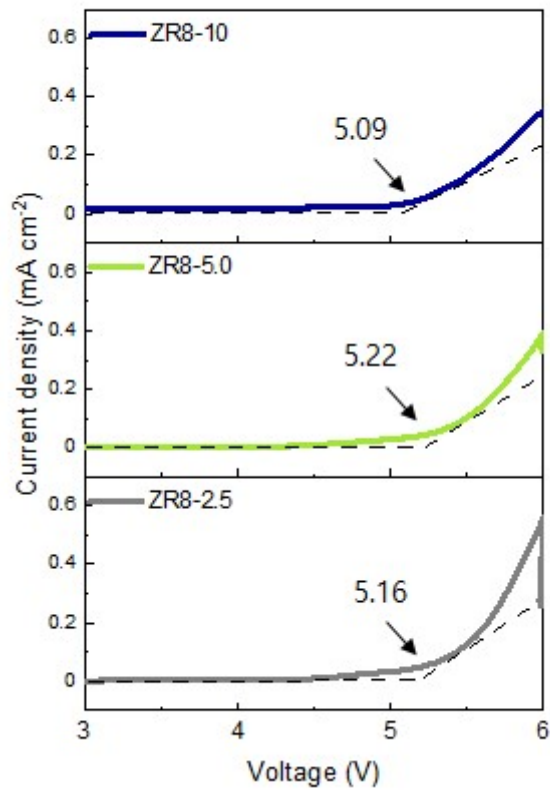


Fig. S12. LSV data for ZR8-2.5, ZR8-5, ZR8-10 of coin cell [SS|ZR8-CPE|Li] @60 °C.

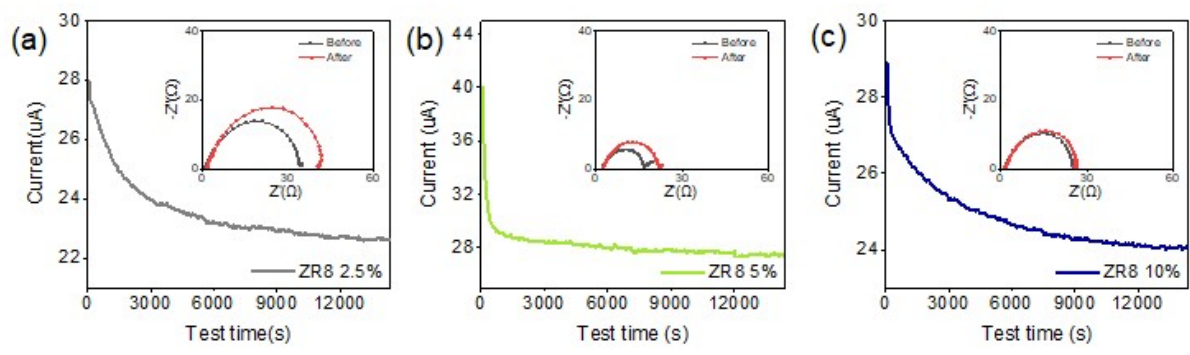


Fig. S13. Current-time profile for ZR8-CPEs for various ZR8 content of (a) 2.5%, (b) 5%, and (c) 10% of coin cell [Li|ZR8-CPE|Li] @60 °C with polarization voltage of 10 mV for 14400 s (inset: the EIS before and after polarization).

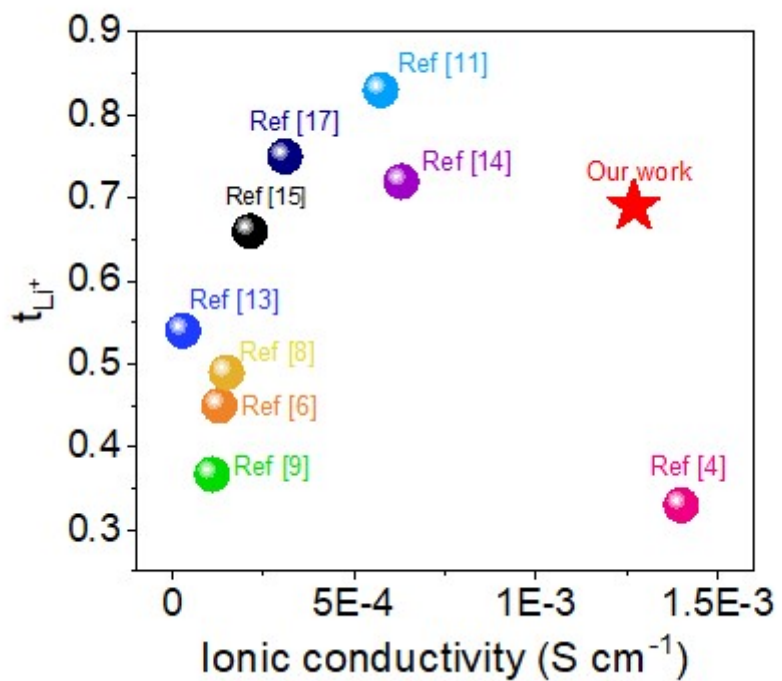


Fig. S14. Comparison of Lithium transference number and ionic conductivity at 60 °C with previously published articles.^{4, 8, 9, 11, 13-15, 17}

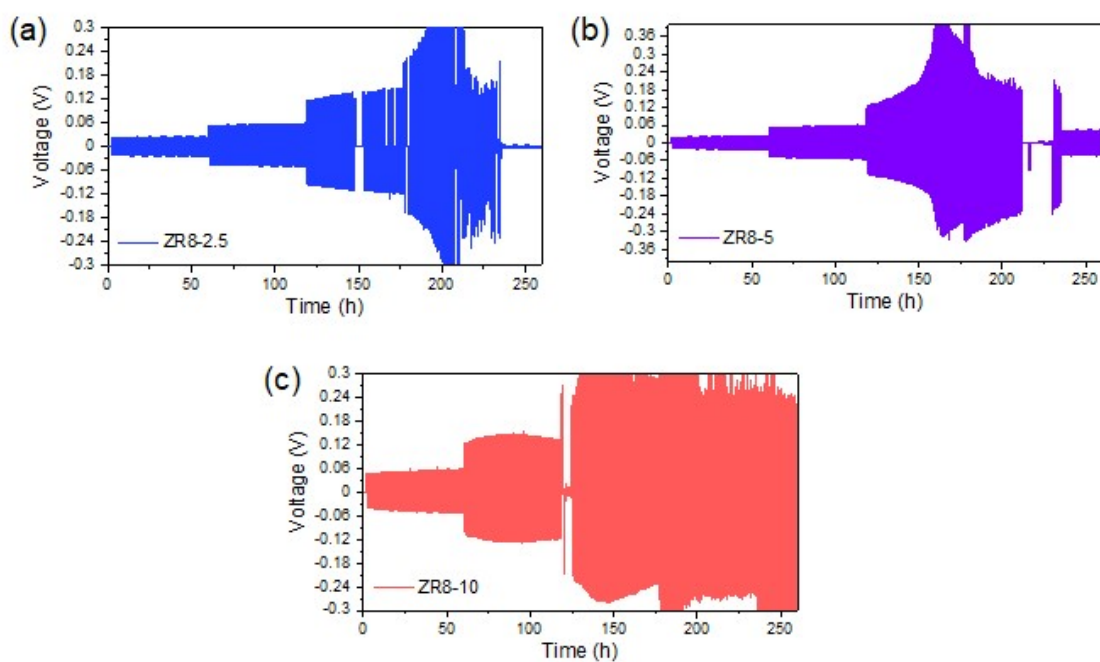


Fig. S15. Electrochemical performance of Li-stripping cycling in the [Li|electrolyte|Li] at different density of $50\text{--}300 \mu\text{A cm}^{-2}$ for 300 cycles at 60°C (a) ZR8-2.5, (b) ZR8-5, and (c) ZR8-10.

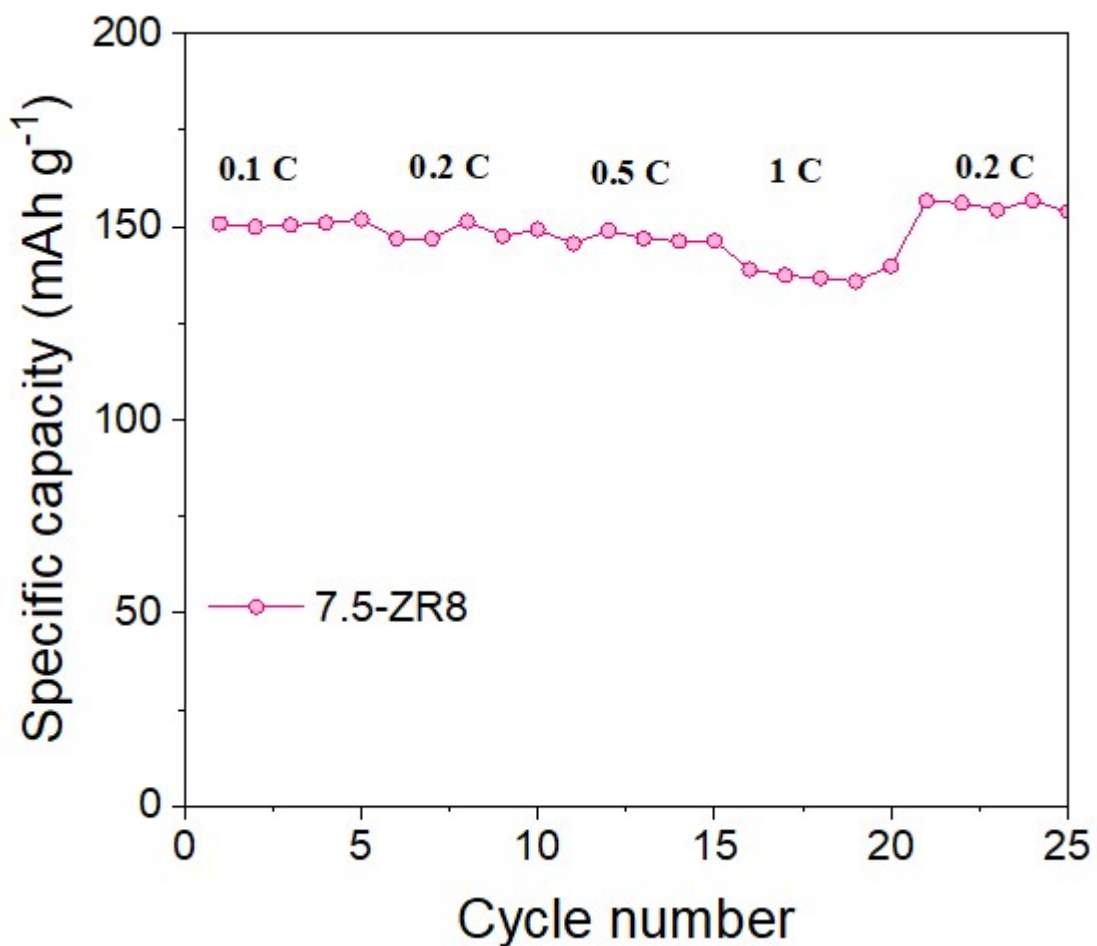


Fig. S16. ZR8-7.5 capacity with LFP at different current density.

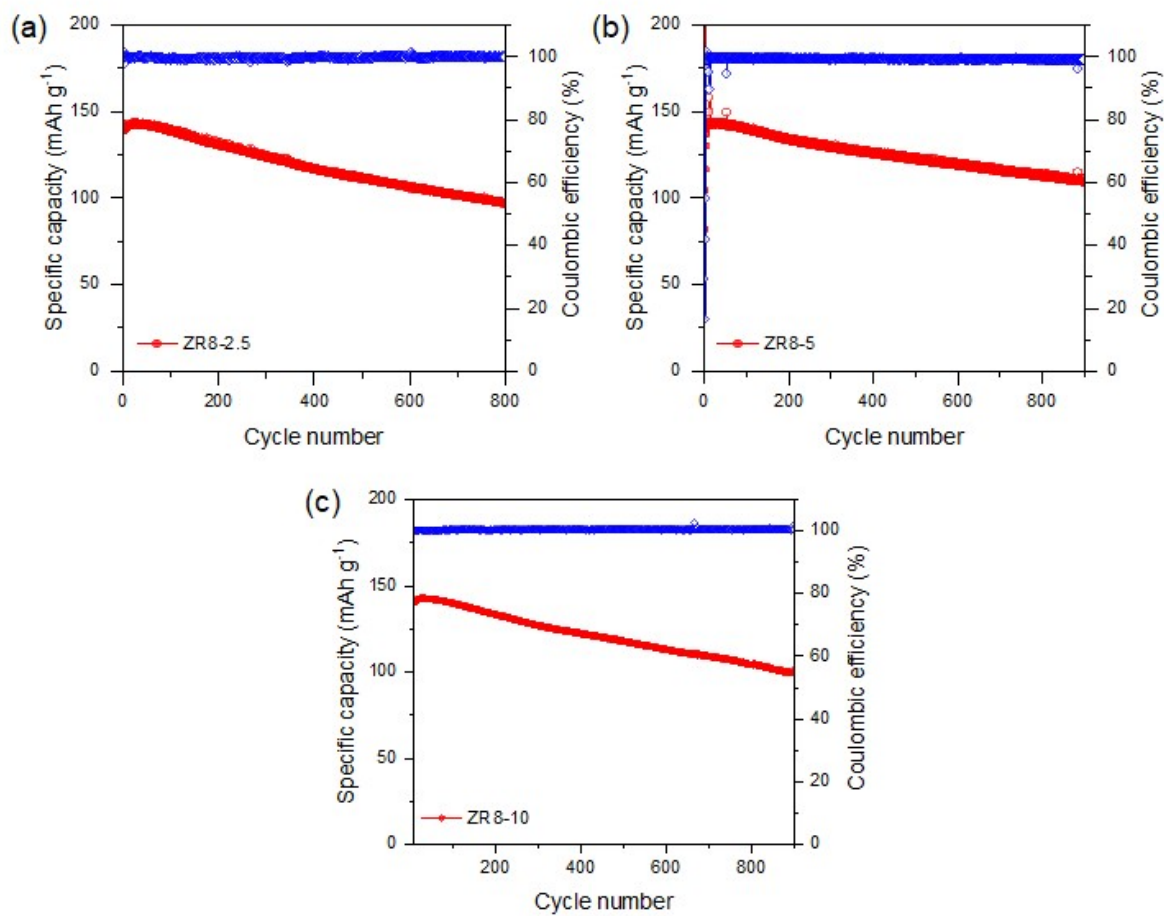


Fig. S17. Cycling performance of ZR8-CPEs for 800 cycles at 0.5 C using coin cell [Li|ZR8-CPE|LFP] at 60 °C (a) ZR8-2.5, (b) ZR8-5, and (c) ZR8-10.

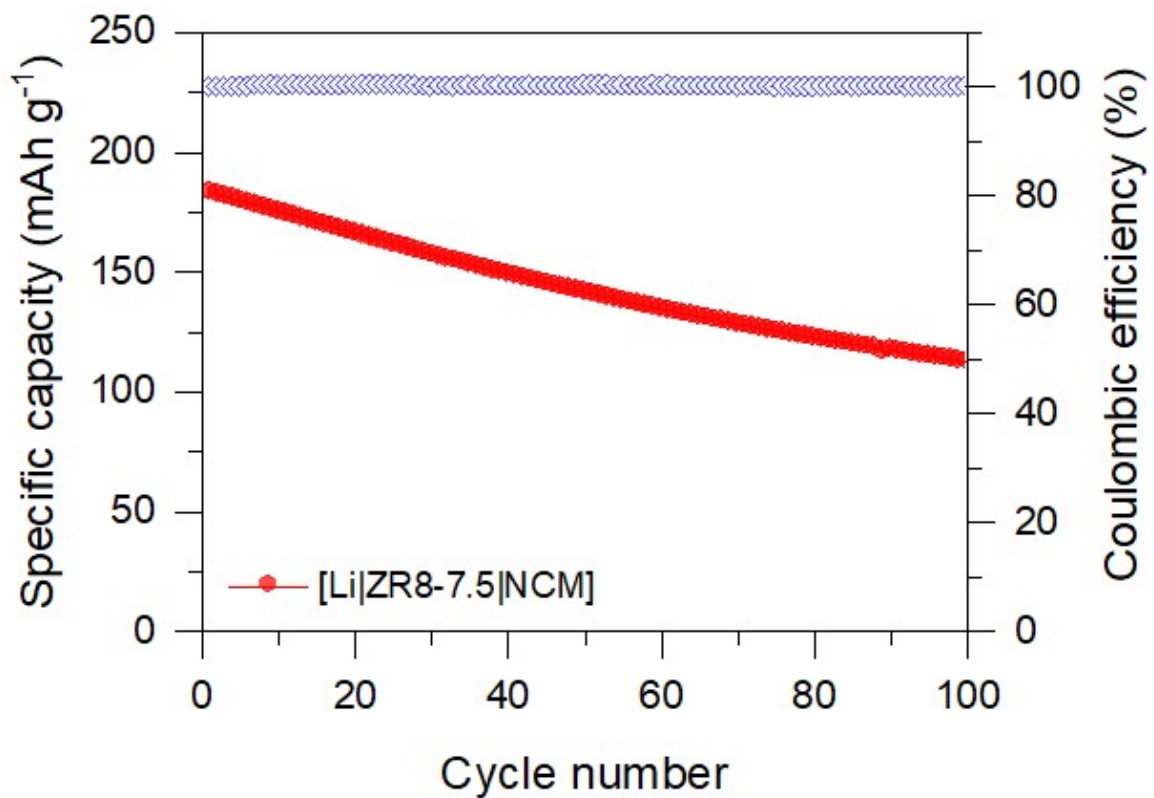


Fig. S18. Cycling performance of ZR8-7.5 CPE for 100 cycles at 0.1 C using coin cell [Li|electrolyte|NCM811] at 60 °C.

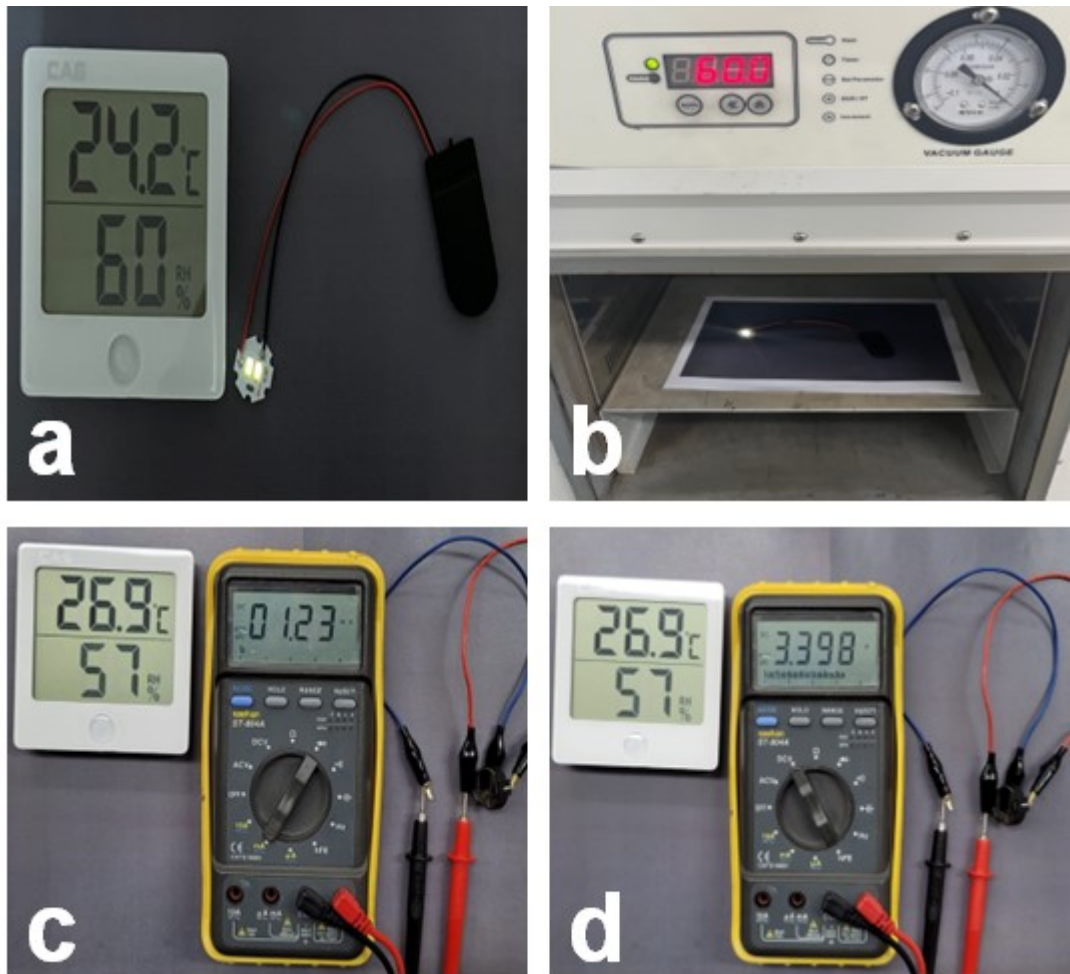


Fig. S19. (a) The practical utility of a coin cell based on ZR8-7.5 CPE for lighting a LED at room temperature, (b) The practical utility of a coin cell based on ZR8-7.5 electrolyte for lighting a LED at 60 °C, (c) The picture of ZR8-CPE coin cell with multimeter during the measurement of current at room temperature, and (d) The picture of ZR8-CPE coin cell with multimeter during the measurement of voltage at room temperature.

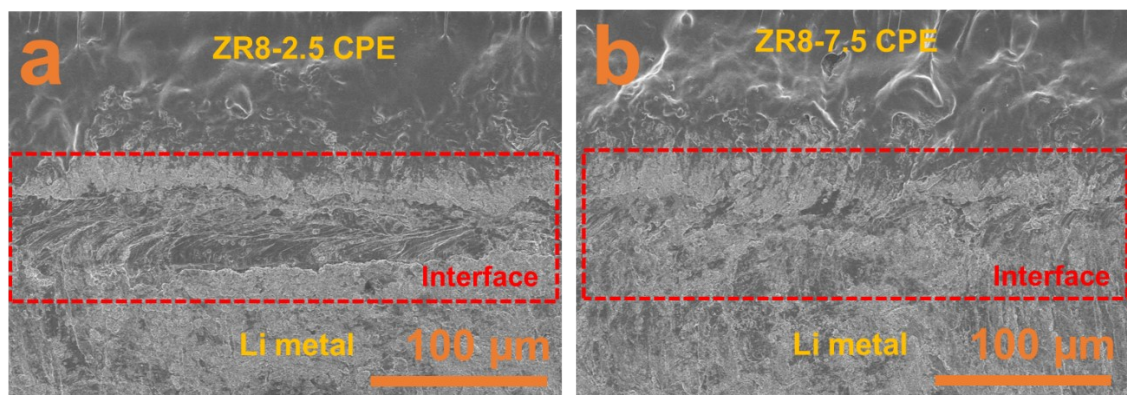


Fig. S20. SEM images of the (a) after cycling [Li|ZR8-2.5|LFP] cell, and (b) [Li|ZR8-7.5|LFP] for 800 cycles.

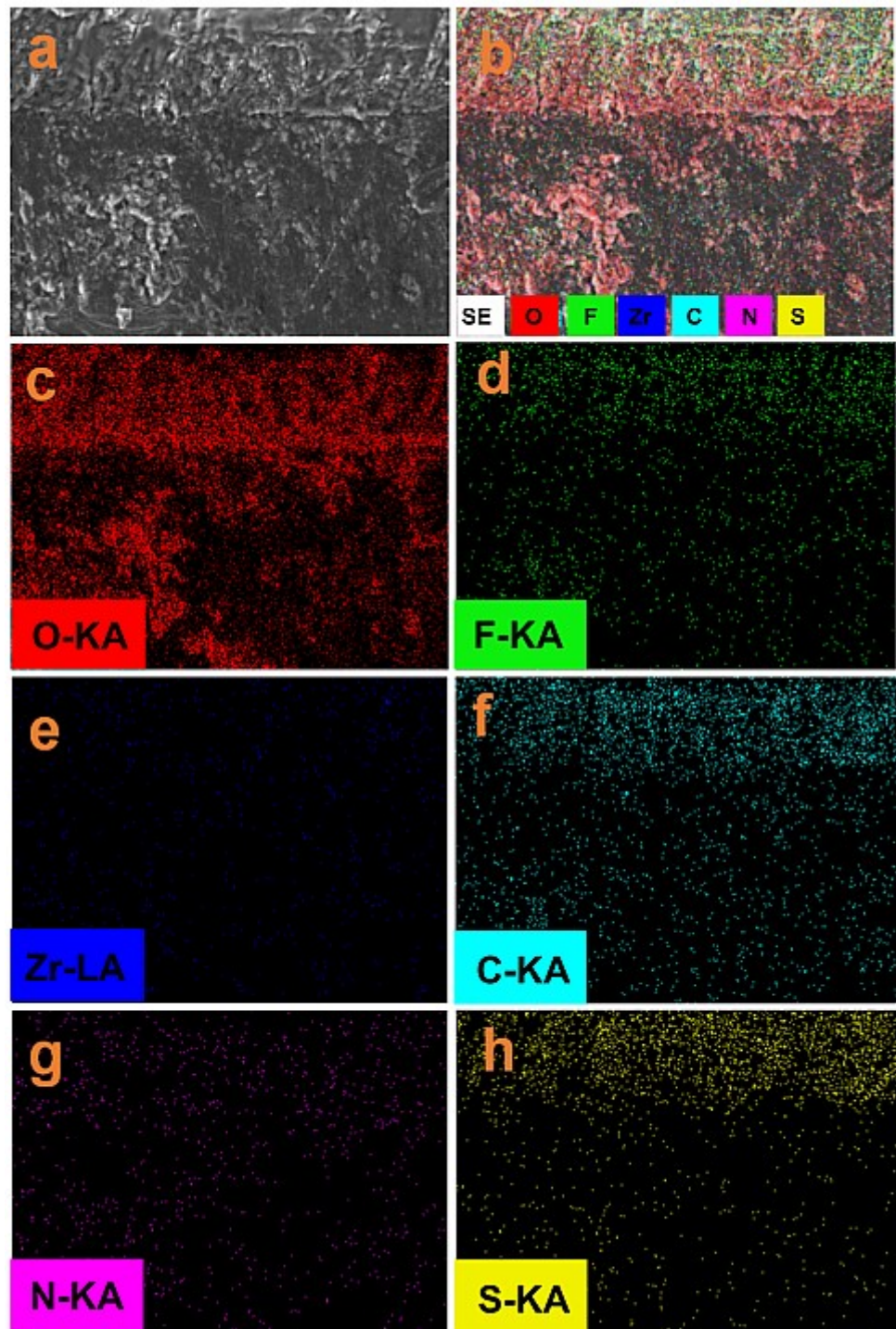


Fig. S21. The FE-SEM image and SEM-EDX mapping of ZR8-7.5 after cycling for 800 cycles
(a) SEM image, (b) overall mapping, (c) O (d) F (e) Zr, (f) C, (g) N, and (h) S element.

References

1. J. Xu, J. Liu, Z. Li, X. Wang, Y. Xu, S. Chen and Z. Wang, *New J Chem*, 2019, **43**, 4092-4099.
2. Shalu, V. K. Singh and R. K. Singh, *Journal of Materials Chemistry C*, 2015, **3**, 7305-7318.
3. S. K. Chaurasia, A. L. Saroj, Shalu, V. K. Singh, A. K. Tripathi, A. K. Gupta, Y. L. Verma and R. K. Singh, *AIP Advances*, 2015, **5**, 077178.
4. C. Li, Y. Huang, X. Feng, Z. Zhang, H. Gao and J. Huang, *J. Colloid Interface Sci*, 2021, **594**, 1-8.
5. J. Wu, J. Chen, X. Wang, A. Zhou and Z. Yang, *Mater. Chem. Front.*, 2021, **5**, 7767-7777.
6. H. Chen, D. Adekoya, L. Hencz, J. Ma, S. Chen, C. Yan, H. Zhao, G. Cui and S. Zhang, *Advanced Energy Materials*, 2020, **10**.
7. Z. Guo, Y. Pang, S. Xia, F. Xu, J. Yang, L. Sun and S. Zheng, *Adv. Sci*, 2021, **8**, 2100899.
8. Z. Xu, T. Yang, X. Chu, H. Su, Z. Wang, N. Chen, B. Gu, H. Zhang, W. Deng, H. Zhang and W. Yang, *Appl. Mater. Interfaces*, 2020, **12**, 10341-10349.
9. X. Tan, Y. Wu, W. Tang, S. Song, J. Yao, Z. Wen, L. Lu, S. V. Savilov, N. Hu and J. Molenda, *Nanomaterials*, 2020, **10**, 157.
10. X. Shen, R. Li, H. Ma, L. Peng, B. Huang, P. Zhang and J. Zhao, *Solid State Ion.*, 2020, **354**, 115412.
11. H. Jamal, F. Khan, H. Lim and J. H. Kim, *SM&T*, 2023, **35**, e00548.
12. Q. Liang, L. Chen, J. Tang, X. Liu, J. Liu, M. Tang and Z. Wang, *Energy Stor. Mater.*, 2023, **55**, 847-856.
13. W. Wen, Q. Zeng, P. Chen, X. Wen, Z. Li, Y. Liu, J. Guan, A. Chen, W. Liu and L. Zhang, *Nano Res.*, 2022, **15**, 8946-8954.
14. H. Huo, B. Wu, T. Zhang, X. Zheng, L. Ge, T. Xu, X. Guo and X. Sun, *Energy Storage Materials*, 2019, **18**, 59-67.
15. D. Han, Z. Zhao, Z. Xu, H. Wang, Z. He, H. Wang, J. Shi and L. Zheng, *ACS Appl. Energy Mater.*, 2022, **5**, 8973-8981.
16. T. Wei, Z. Wang, M. Zhang, Q. Zhang, J. Lu, Y. Zhou, C. Sun, Z. Yu, Y. Wang, M. Qiao and S. Qin, *Mater. Today Commun.*, 2022, **31**, 103518.
17. X. Wu, K. Chen, Z. Yao, J. Hu, M. Huang, J. Meng, S. Ma, T. Wu, Y. Cui and C. Li, *J. Power Sources*, 2021, **501**, 229946.
18. J. Hu, W. Wang, X. Zhu, S. Liu, Y. Wang, Y. Xu, S. Zhou, X. He and Z. Xue, *J. Membr. Sci*, 2021, **618**, 118697.
19. A. Li, X. Liao, H. Zhang, L. Shi, P. Wang, Q. Cheng, J. Borovilas, Z. Li, W. Huang, Z. Fu, M. Dontigny, K. Zaghib, K. Myers, X. Chuan, X. Chen and Y. Yang, *Adv Mater*, 2020, **32**, 1905517.
20. R. Fang, B. Xu, N. S. Grundish, Y. Xia, Y. Li, C. Lu, Y. Liu, N. Wu and J. B. Goodenough, *Angew. Chem. Int. Ed.*, 2021, **60**, 17701-17706.
21. H. Jamal, F. Khan, H.-R. Si and J. H. Kim, *J. Mater. Chem. A*, 2021, **9**, 27304-27319.
22. D. Lin, W. Liu, Y. Liu, H. R. Lee, P.-C. Hsu, K. Liu and Y. Cui, *Nano Letters*, 2016, **16**, 459-465.

23. J. Yu, C. Wang, S. Li, N. Liu, J. Zhu and Z. Lu, *Small*, 2019, **15**, 1902729.
24. Z. Wan, D. Lei, W. Yang, C. Liu, K. Shi, X. Hao, L. Shen, W. Lv, B. Li, Q.-H. Yang, F. Kang and Y.-B. He, *Adv. Funct. Mater.*, 2019, **29**, 1805301.
25. K. Pan, L. Zhang, W. Qian, X. Wu, K. Dong, H. Zhang and S. Zhang, *Adv Mater*, 2020, **32**, 2000399.
26. W. Tang, S. Tang, X. Guan, X. Zhang, Q. Xiang and J. Luo, *Adv. Funct. Mater.*, 2019, **29**, 1900648.